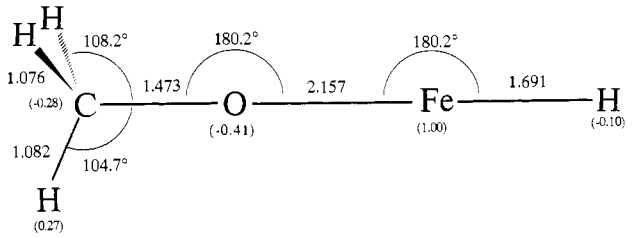

8

[- 15 kcal/mol]

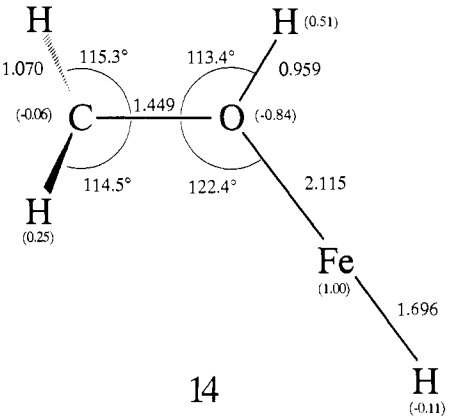

14

[- 12 kcal/mol]

one would expect that collisional activation inter alia gives rise to an abundant FeH^+ signal, this is not the case (Table III). Rather, the CA mass spectrum of system VII ($HCOCH_2OH$) can be explained by a 5:1 mixture of the two isomers **3** and **7** (H_3C–Fe–OH^+ and H_2C=Fe—OH_2^+, respectively). Obviously, quite a complex rearrangement of **14** to the thermochemically much more stable isomers **3** and **7** occurs by mechanisms which, for the time being, are not fully understood.

Finally, we would like to point out that the various $[Fe,C,H_4,O]^+$ isomers described in this section can be assigned to four different classes of bonding types. As indicated by the data given in Table V, while the d-electron population at the iron atom is almost unchanged for all isomers, we obtain quite pronounced differences for the s- and p-electron populations.

In complex **4** there is a clear σ-interaction from the doubly occupied orbital at the oxygen atom with the empty p_σ orbital of iron. The s-occupancy is unchanged.

For the isomers **8** and **14** we observe the same populations as for the H–Fe–OH^+ complex, which is given as a reference; here the ss- and sp-overlap lead to a lowering of the s-population and the donation of 0.18 electron in the p_σ of iron. In complexes **1** and **3**, the iron is formally oxidized, as ca. 0.8 electron from the s orbital is removed; a modest π-donation (ca. 0.1 electron) in the p_π orbital occurs.

The population of **7** differs from all bonding types considered. Donation in the π- as well as σ-system is observed. This is in accordance with both the Fe–O and Fe–C bond lengths of **7**.

Acknowledgment. We gratefully acknowledge financial support of our work by the Deutsche Forschungsgemeinschaft, Volkswagen-Stiftung, Fonds der Chemischen Industrie, and Gesellschaft von Freunden der Technischen Universität Berlin. Constructive comments and suggestions by the reviewers are appreciated.

Registry No. **3**, 138259-33-3; **4**, 138259-34-4; **7**, 138259-35-5; **8**, 138259-36-6; **12**, 90143-30-9; **13**, 126492-96-4; **14**, 138259-37-7; c-C_3H_6, 75-19-4; CH_3SO_2OH, 75-75-2; CH_3OH, 67-56-1; $HCOOCH_3$, 107-31-3; CH_4, 74-82-8; n-C_3H_7OH, 71-23-8; $HCOCH_2OH$, 141-46-8; CH_3COOH, 64-19-7; $Fe(CO)_5$, 13463-40-6; FeO^+, 12434-84-3.

Atomic Scale Imaging of Alkanethiolate Monolayers at Gold Surfaces with Atomic Force Microscopy

Carla A. Alves, Earl L. Smith, and Marc D. Porter*

Contribution from Ames Laboratory—U.S. Department of Energy and the Department of Chemistry, Iowa State University, Ames, Iowa 50011. *Received September 3, 1991*

Abstract: Monolayer films formed by the chemisorption of alkanethiols ($CH_3(CH_2)_nSH$, n = 1-17) at epitaxially grown Au(111) films were examined using atomic force microscopy (AFM). Atomically resolved images were found for films with $n \geq 4$, directly revealing for the first time the arrangement of the alkyl chain structure. All of the images exhibit a periodic hexagonal pattern of equivalent spacings (e.g., respective nearest- and next-nearest-neighbor distances of 0.52 ± 0.03 and 0.90 ± 0.04 nm for n = 17 and 0.51 ± 0.02 and 0.92 ± 0.06 nm for n = 5). These spacings agree well with the analogous 0.50- and 0.87-nm distances of a $(\sqrt{3} \times \sqrt{3})R30°$ adlayer on a Au(111) lattice, the two-dimensional arrangement reported in recent diffraction[1-3] and scanning tunneling microscopy[4,5] studies. In some instances, images with the above spacings were observed to extend continuously over areas as large as 100 nm^2, suggesting the potential of AFM to reveal both the short- and long-range order of the alkyl chains of these and other model interfacial structures. The implications of these findings, including the inability to obtain well-resolved images for films with $n \leq 3$, are examined in the context both of the current structural descriptions of alkanethiolate monolayers and of general issues related to imaging organic films with AFM.

Introduction

The atomic force microscope[6] (AFM) and its predecessor, the scanning tunneling microscope[7] (STM), have emerged as powerful tools for imaging semiconductor,[8] metallic,[9] organic,[10] and biological[11] surfaces with atomic scale resolution in environments ranging from ultrahigh vacuum to aqueous solutions. We have recently begun to assess the applicability of both techniques for imaging model organic interfacial systems, such as the alkanethiolate[12] monolayers that form on gold surfaces. The goal is to

* To whom correspondence should be addressed.

(1) Chidsey, C. E. D.; Liu, G.-Y.; Rowntree, P.; Scoles, G. *J. Chem. Phys.* **1989**, *91*, 4421-3.

(2) (a) Strong, L.; Whitesides, G. M. *Langmuir* **1988**, *4*, 546-58. (b) For additional details: Chidsey, C. E. D.; Loiacono, D. M. *Langmuir* **1990**, *6*, 682-91.

(3) Samant, M. G.; Brown, C. A.; Gordon, J. G., II. *Langmuir* **1991**, *7*, 437-9.

0002-7863/92/1514-1222$03.00/0

develop detailed descriptions of the short- and long-range packing arrangements of these monolayers that will serve as a basis for correlating the interfacial microstructure with macroscopic observables (e.g., wettability[13] and electron-transfer properties[2b,14]). In an earlier effort,[4] we demonstrated that STM can reveal the two-dimensional arrangement of alkanethiolate monolayers at gold—observations attributed to electrons tunneling between the STM tip and the gold surface through the thiolate head group. As our explorations of the capabilities of STM and AFM progressed, we discovered that it was also possible to image these monolayers using AFM under ambient conditions. This paper reports the results of our findings.

In the following sections, we present the first atomically resolved AFM images of monolayers formed by the chemisorption of alkanethiols ($CH_3(CH_2)_nSH$) at epitaxially grown Au(111). To set a foundation for the discussion of our images, we first describe the conditions that lead to the observation of atomic structure using AFM. This section also contrasts the ability to image these adsorbates using AFM and STM. Next, we present an atomically resolved AFM image of our mica-supported gold films. This image defines the (111) texture of the uncoated gold surfaces and functions as a reference for comparison to the images of the alkanethiolate-coated gold samples. The AFM images of the thiolate monolayers are then presented. Though difficult to define fully, we believe these images arise from interactions between the AFM tip and the alkyl chains of the resulting gold(I) alkanethiolate monolayer. Recent literature precedents[10a,11a,15-17] as well as results from attempts to image alkanethiolate monolayers of varied chain length ($n = 1$–17) are used to support this contention. For $n \geq 4$, an image that corresponds to a $(\sqrt{3} \times \sqrt{3})R30°$ adlayer was found, the same two-dimensional arrangement found for these monolayers using diffraction[1-3] and STM[4,5] techniques. Images with a well-defined periodicity have not yet been observed for monolayers with $n \leq 3$. We conclude with a brief assessment of our images in the context of established and emerging structural descriptions of these monolayers.[12-14,18,19]

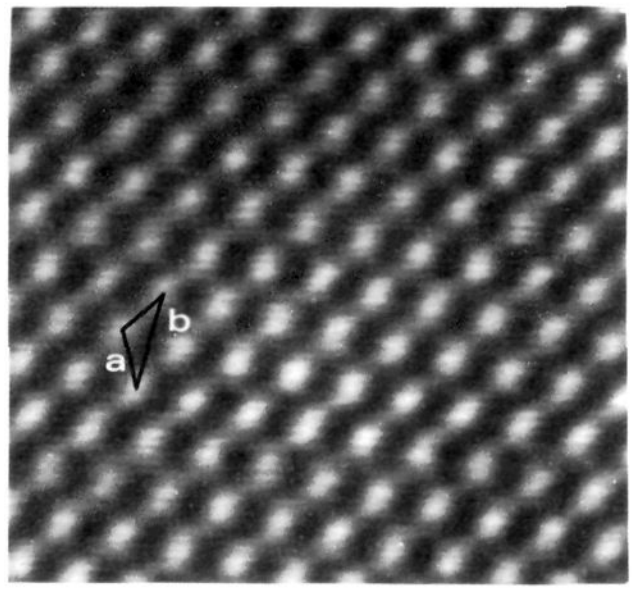

Figure 1. AFM image of uncoated, epitaxially grown Au(111) on mica covering 3.02 nm × 3.02 nm. The image was collected in a constant-force mode and was lightly filtered using an XY spectrum filter. The average nearest-neighbor spacing represented by line a equals 0.29 ± 0.03 nm, and the next-nearest-neighbor spacing represented by line b is 0.50 ± 0.04 nm.

Experimental Section

Substrate Preparation. Gold substrates with a predominantly (111) crystallinity were prepared by the resistive evaporation of 300 nm of gold onto freshly cleaved green mica sheets (Asheville-Schoonmaker, Newport News, VA) at a rate of 0.3 nm/s. Immediately prior to gold deposition,

(4) Widrig, C. A.; Alves, C. A.; Porter, M. D. *J. Am. Chem. Soc.* **1991**, *113*, 2805–10.

(5) The $(\sqrt{3} \times \sqrt{3})R30°$ adlayer structure has also been observed for monolayers formed by the adsorption of 4-aminothiophenol at Au(111). Kim, Y.-T.; McCarley, R. L.; Bard, A. J. Private communication.

(6) Binnig, G.; Quate, C. F.; Gerber, Ch. *Phys. Rev. Lett.* **1986**, *456*, 930–3.

(7) Binnig, G.; Rohrer, H. *Surf. Sci.* **1983**, *126*, 236–44.

(8) See for example: (a) Becker, R. S.; Swartzentruber, B. S.; Vickers, J. S. *J. Vac. Sci. Technol. A* **1988**, *6*, 472–7. (b) Köhler, U.; Jusko, O.; Pietsch, G.; Müller, B.; Henzler, M. *Surf. Sci.* **1991**, *248*, 321–31. (c) Whitman, L. J.; Stroscio, J. A.; Dragoset, R. A.; Celotta, R. J. *J. Vac. Sci. Technol. B* **1991**, *9*, 770–4. (d) Chang, H.; Bard, A. J.; *J. Am. Chem. Soc.* **1991**, *113*, 5588–96.

(9) See for example: (a) Manne, S.; Butt, H. J.; Gould, S. A. C.; Hansma, P. K. *Appl. Phys. Lett.* **1990**, *56*, 1758–9. (b) Manne, S.; Hansma, P. K.; Massie, J.; Elings, V. B.; Gewirth, A. A. *Science* **1991**, *251*, 183–6. (c) Weisenhorn, A. L.; Henriksen, P. N.; Chu, H. T.; Ramsier, R. D.; Reneker, D. H. *J. Vac. Sci. Technol. B* **1991**, *9*, 1333–5. (d) Hallmark, V. M.; Chiang, S.; Rabolt, J. F.; Swalen, J. D.; Wilson, R. J. *Phys. Rev. Lett.* **1987**, *59*, 2879–82. (e) Emch, R.; Nogami, J.; Dovek, M. M.; Lang, C. A.; Quate, C. F. *J. Appl. Phys.* **1989**, *65*, 79–84. (f) Yau, S.-L.; Gao, X.; Chang, S.-C.; Schardt, B. C.; Weaver, M. J. *J. Am. Chem. Soc.* **1991**, *113*, 6049–56. (g) Schardt, B. C.; Yau, S.-L.; Rinaldi, F. *Science* **1989**, *243*, 1050–3. (h) Ogletree, D. F.; Hwang, R. Q.; Zeglinski, D. M.; Vazquez-de-Parga, A. L.; Somorjai, G. A.; Salmeron, M. *J. Vac. Sci. Technol. B* **1991**, *9*, 886–90. (i) Magnussen, O. M.; Hotlos, J.; Beitel, G.; Kolb, D. M.; Behm, R. J. *J. Vac. Sci. Technol. B* **1991**, *9*, 969–75.

(10) See for example: (a) Meyer, E.; Howald, L.; Overney, R. M.; Heinzelmann, H.; Frommer, J.; Güntherodt, H.-J.; Wagner, T.; Schier, H.; Roth, S. *Nature* **1991**, *349*, 398–400. (b) Drake, B.; Prater, C. B.; Weisenhorn, A. L.; Gould, S. A. C.; Albrecht, T. R.; Quate, C. F.; Cannell, D. S.; Hansma, H. G.; Hansma, P. K. *Science* **1989**, *243*, 1586–9. (c) Mate, C. M.; Lorenz, M. R.; Novotny, V. J. *J. Chem. Phys.* **1989**, *90*, 7550–5. (d) Smith, D. P. E.; Hörber, J. K. H.; Binnig, G.; Nejoh, H. *Nature* **1990**, *344*, 641–4. (e) Ohtani, H.; Wilson, R. J.; Chiang, S.; Mate, C. M. *Phys. Rev. Lett.* **1988**, *60*, 2398–2401. (f) Hallmark, V. M.; Chiang, S.; Wöll, Ch. *J. Vac. Sci. Technol. B* **1991**, *9*, 1111–4. (g) Magonov, S. N.; Kempf, S.; Rotter, H.; Cantow, H.-J. *Synth. Met.* **1991**, *40*, 73–86.

(11) See for example: (a) Weisenhorn, A. L.; Egger, M.; Ohnesorge, F.; Gould, S. A. C.; Heyn, S.-P.; Hansma, H. G.; Sinsheimer, R. L.; Gaub, H. E.; Hansma, P. K. *Langmuir* **1991**, *7*, 8–12. (b) Lin, J. N.; Drake, B.; Lea, A. S.; Hansma, P. K.; Andrade, J. D. *Langmuir* **1990**, *6*, 509–11. (c) Egger, M.; Ohnesorge, F.; Weisenhorn, A. L.; Heyn, S. P.; Drake, B.; Prater, C. B.; Gould, S. A. C.; Hansma, P. K.; Gaub, H. E. *J. Struct. Biol* **1990**, *103*, 89–94. (d) Gould, S. A. C.; Drake, B.; Prater, C. B.; Weisenhorn, A. L.; Manne, S.; Hansma, H. G.; Hansma, P. K.; Massie, J.; Longmire, M.; Elings, V.; Northern, B. D.; Mukergee, B.; Peterson, C. M.; Stoeckenius, W.; Albrecht, T. R.; Quate, C. F. *J. Vac. Sci. Technol. A* **1990**, *8*, 369–73. (e) Beebe, T. P. Jr.; Wilson, T. E.; Ogletree, D. F.; Katz, J. E.; Balhorn, R.; Salmeron, M. B.; Siekhaus, W. J. *Science* **1989**, *243*, 370–2. (f) Salmeron, M.; Beebe, T.; Odriozola, J.; Wilson, T.; Ogletree, D. F.; Siekhaus, W.; *J. Vac. Sci. Technol. A.* **1990**, *8*, 635–41.

(12) Evidence that these monolayers form as the corresponding thiolates at Au is given in: (a) Widrig, C. A.; Chung, C.; Porter, M. D. *J. Electroanal. Chem.* **1991**, *310*, 335–59. (b) Bryant, M. A.; Pemberton, J. E. *J. Am. Chem. Soc.* **1991**, *113*, 8284–93. (c) Bain, C. D.; Biebuyck, H. A.; Whitesides, G. M. *Langmuir* **1989**, *5*, 723–7.

(13) (a) Whitesides, G. M.; Laibinis, P. E. *Langmuir* **1990**, *6*, 87–96. (b) Nuzzo, R. G.; Dubois, L. H.; Allara, D. L. *J. Am. Chem. Soc.* **1990**, *112*, 558–69. (c) Dubois, L. H.; Zegarski, B. R.; Nuzzo, R. G. *J. Am. Chem. Soc.* **1990**, *112*, 570–9.

(14) (a) Porter, M. D.; Bright, T. B.; Allara, D. L.; Chidsey, C. E. D. *J. Am. Chem. Soc.* **1987**, *109*, 3559–69. (b) Li, T. T.-T.; Weaver, M. J. *J. Am. Chem. Soc.* **1984**, *106*, 6107–8. (c) Sabatani, E.; Rubinstein, I. *J. Phys. Chem.* **1987**, *91*, 6663–9. (d) Finklea, H. O.; Snider, D. A.; Fedyk, J. *Langmuir* **1990**, *6*, 371–6. (e) De Long, H. C.; Buttry, D. A. *Langmuir* **1990**, *6*, 1319–22. (f) Chidsey, C. E. D. *Science* **1991**, *251*, 919–22. (g) Creager, S. E.; Rowe, G. K. *Anal. Chim. Acta* **1991**, *246*, 233–9. (h) Tarlov, M. J.; Bowden, E. F. *J. Am. Chem. Soc.* **1991**, *113*, 1847–9.

(15) Blackman, G. S.; Mate, C. M.; Philpott, M. R. *Phys. Rev. Lett.* **1990**, *65*, 2270–3.

(16) Burnham, N. A.; Dominguez, D. D.; Mowery, R. L.; Colton, R. J. *Phys. Rev. Lett.* **1990**, *64*, 1931–4.

(17) Novotny, V.; Swalen, J. D.; Rabe, J. P. *Langmuir* **1989**, *5*, 485–9.

(18) (a) Nuzzo, R. G.; Zegarski, B. R.; Dubois, L. H. *J. Am. Chem. Soc.* **1987**, *109*, 733–40. (b) Ulman, A.; Eilers, J. E.; Tillman, N. *Langmuir* **1989**, *5*, 1147–52. (c) Bain, C. D.; Troughton, E. B.; Tao, Y.-T.; Evall, J.; Whitesides, G. M.; Nuzzo, R. G. *J. Am. Chem. Soc.* **1989**, *111*, 321–35. (d) Nuzzo, R. G.; Korenic, E. M.; Dubois, L. H. *J. Chem. Phys.* **1989**, *93*, 767–73. (e) Nuzzo, R. G.; Allara, D. L. *J. Am. Chem. Soc.* **1983**, *105*, 4481–3. (f) Evans, S. D.; Urankar, E.; Ulman, A.; Ferris, N. *J. Am. Chem. Soc.* **1991**, *113*, 4121–31.

(19) Walczak, M. M.; Popenoe, D. D.; Deinhammer, R. S.; Lamp, B. D.; Chung, C.; Porter, M. D. *Langmuir* **1991**, *7*, 2687–93.

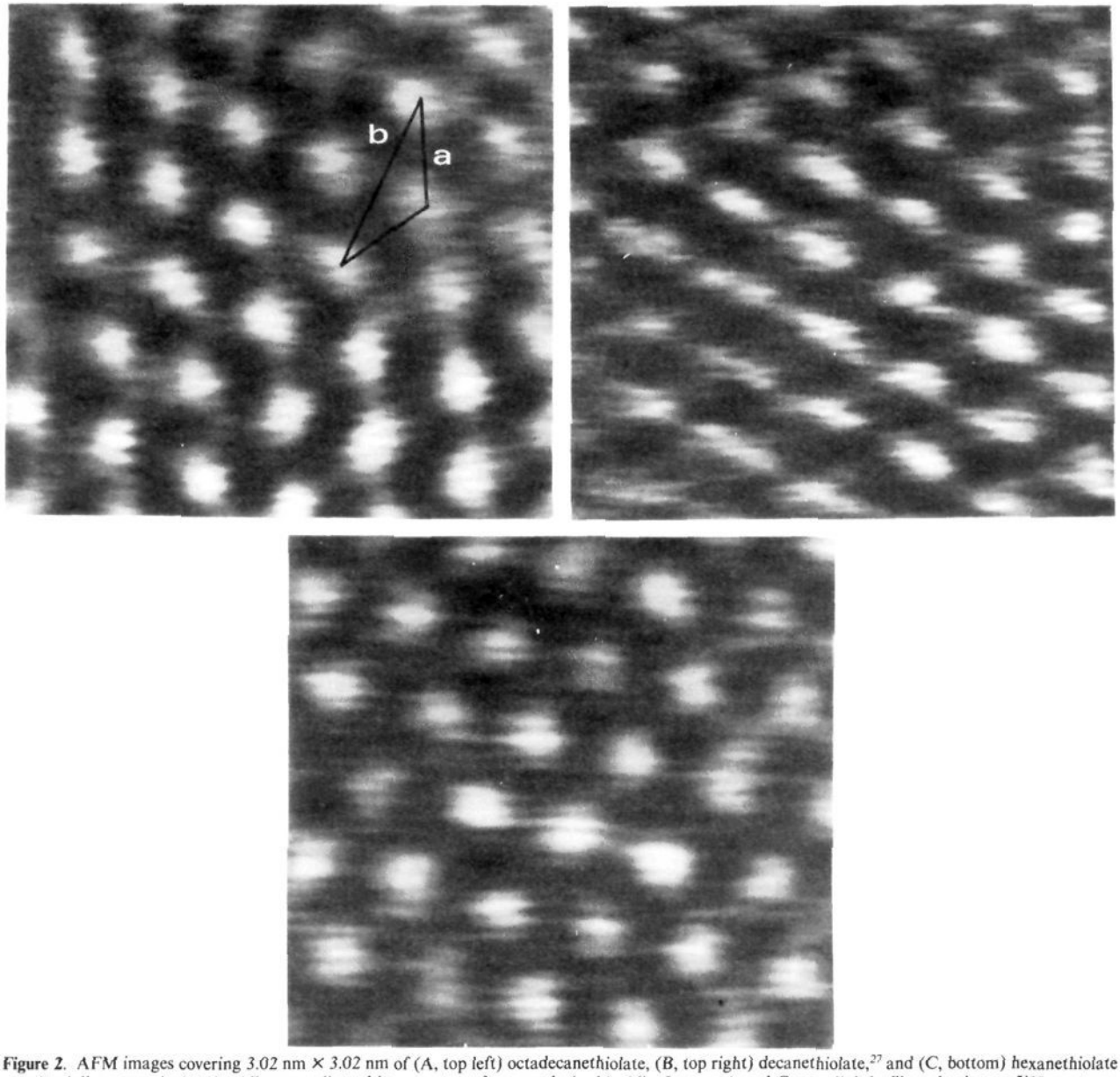

Figure 2. AFM images covering 3.02 nm × 3.02 nm of (A, top left) octadecanethiolate, (B, top right) decanethiolate,[27] and (C, bottom) hexanethiolate at epitaxially grown Au(111). All were collected in a constant-force mode (~10 nN). Images A and C were lightly filtered using an XY spectrum filter, and B was low-pass filtered. The nearest- and next-nearest-neighbor spacings are represented in A by the black lines, *a* and *b*, respectively. Average spacings for distances in each of the images: (A) $a = 0.52 \pm 0.03$ nm, $b = 0.90 \pm 0.04$ nm; (B) $a = 0.50 \pm 0.02$, $b = 0.91 \pm 0.04$ nm; (C) $a = 0.51 \pm 0.02$, $b = 0.92 \pm 0.06$ nm. These spacings correspond to a $(\sqrt{3} \times \sqrt{3})R30°$ adsorbate overlayer on Au(111).

the mica sheets were heated in the vacuum chamber for ~1 h at 250–300 °C. During deposition, the pressure in a cryogenically pumped Edwards 306A vacuum chamber (Fairfield, CA) was held at $\sim 2 \times 10^{-6}$ Torr. Subsequently, the gold-coated mica was allowed to cool radiatively to below 70 °C before back-filling the chamber with dry nitrogen and removing the substrates. The substrates were then immediately immersed into the thiol solutions.

Previous macroscopic level characterizations of our evaporated gold films using STM[4] indicate that the gold films are composed of ~300-nm-wide crystallites that are separated by relatively deep grain boundaries. The roughness factor of the gold substrates, given by the electrochemically determined area[20] divided by the geometric area, equals 1.1 ± 0.1.[21] At a microscopic level, the surfaces of the uncoated gold films are strongly (111) textured[21] (>95%), based on comparisons of the voltammetric curves for the underpotential deposition of Pb(II) to literature data at single-crystal gold electrodes.[22] Images from STM[4] routinely exhibit the 0.29-nm interatomic spacing of Au(111). The latter findings are in general agreement with earlier STM[9d,e] and AFM[9a,b] reports as well as electron diffraction[9d,23,24] studies.

Monolayer Film Preparation. Alkanethiolate monolayers were prepared by the chemisorption of the corresponding thiol on gold from ~1 mM ethanolic solutions using previously described protocols.[14a] Upon removal from solution, the samples were rinsed thoroughly with ethanol and dried in air. Varying immersion times from ~2 to 24 h had no observable effect on the resulting AFM images.

Instrumentation. Images were obtained in air using a Digital Instruments Nanoscope II (Santa Barbara, CA). The instrument was equipped with a 0.7-μm AFM scan head. After a sample was loaded, the instrument was allowed to come to thermal equilibrium, which required ~30 min. All images were collected in air with the AFM tip in contact with

(20) The electrochemically determined area is based on measurements of the oxidative desorption of iodine: Rodriguez, J. F.; Mebrahtu, T.; Soriaga, M. P. *J. Electroanal. Chem.* **1987**, *233*, 283–9.

(21) Walczak, M. M.; Alves, C. A.; Deinhammer, R. S.; Lamp, B. D.; Chung, C.; Porter, M. D. Manuscript in preparation.

(22) (a) Schultze, J. W.; Dickertmann, D. *Surf. Sci.* **1976**, *54*, 489–505. (b) Engelsmann, K.; Lorenz, W. J.; Schmidt, E. *J. Electroanal. Chem.* **1980**, *114*, 1–10.

(23) Chidsey, C. E. D.; Loiacono, D. M.; Sleator, T.; Nakahara, S. *Surf. Sci.* **1988**, *200*, 45–66.

(24) Golan, Y.; Margulis, L.; Rubinstein, I. *Surf. Sci.*, submitted for publication.

the sample in the constant force mode (i.e., the height mode of the Nanoscope II). In this mode, the force between the AFM tip and the sample surface is held constant, and the vertical displacements of the sample needed to maintain the preselected force are recorded as the tip rasters across the surface. Triangularly shaped silicon nitride cantilevers with pyramidal tips (Digital Instruments) were used. The force constant of these cantilevers was 0.58 N/m. Images were acquired at a rate of 14–28 lines/s, requiring roughly 15–25 s per image. Imaging forces were ~50 nN, unless otherwise specified. The horizontal displacement of the tip was calibrated using freshly cleaved mica. Images were either smoothed with an eight-point moving-average algorithm (i.e., the low-pass filter utility of the Nanoscope II) or lightly filtered with an XY spectrum filter.

Reagents. Liquid alkanethiols ($CH_3(CH_2)_nSH$) were acquired from several sources (Alfa Products, n = 1; Aldrich, n = 2, 4, 6–8, 15; Eastman Kodak, n = 3, 5, 9, 11; Pfaltz and Bauer, n = 13). Tridecanethiol and pentadecanethiol were synthesized from 1-bromotridecane (Aldrich) and 1-bromopentadecane (Aldrich), respectively, according to previous procedures.[18c] Undecanethiol and heptadecanethiol were gifts from Professor George Whitesides (Department of Chemistry, Harvard University). All of these compounds were purified by passage through a neutral alumina (Aldrich) column prior to use. Octadecanethiol (Aldrich) was recrystallized twice from absolute ethanol.

Results and Discussion

I. General Observations. Using the previously described experimental protocols, we have attempted to image alkanethiolate ($CH_3(CH_2)_nSH$) monolayers at our gold-coated mica substrates for a large range of chain lengths (n = 1–17). Images with atomically resolved features have been observed only for $n \geq 4$. We have yet to obtain well-defined images for $n \leq 3$. As with STM[4], the conditions that yield a well-defined AFM image have been difficult to define. We have found, however, that such images are more readily attained with AFM than with STM. We attribute this primarily to differences in the structural stabilities of the two types of tips. Tips for STM that resolved atomic scale structures functioned effectively for a period between several minutes and a few hours, after which the image gradually or suddenly disappeared. Tips for AFM, on the other hand, were routinely used for several days. We found on numerous occasions that once "in focus", the same area of the sample could be scanned continuously with AFM for several hours with little apparent degradation of the image.

In addition, we have found that the conditions yielding a well-defined image varied somewhat with chain length. Both long-chain structures (e.g., n = 17) and short-chain structures (e.g., n = 5) could effectively be imaged under approximately the same force (~50 nN). However, the long-chain structures were able to withstand greater forces before the image degraded. We attribute the ability of the longer chain structures to withstand greater forces to increasing cohesive interactions between neighboring alkyl chains.[1,13b,14a,18c,d] We have also observed that scanning at low forces (≲20 nN) leads to the loss of image definition. We ascribe this loss of definition to two sources. First, contact between the AFM tip and sample at low forces may be intermittent with the tip repeatedly losing and regaining contact during a scan. Second, the tip may be imaging the extreme outer surface of the chain structure which, at least for longer chain lengths, is disordered with respect to the underlying polymethylene chain. Such disorder reflects the presence of gauche conformational defects at the chain terminus.[25] Further discussion of the implications of our observations is deferred until later.

II. AFM Images of Uncoated Epitaxially Grown Gold. An atomically resolved AFM image of uncoated, epitaxially grown gold is shown in Figure 1. The image encompasses an area slightly larger than 3 nm × 3 nm. This and all other images are given in a top-view presentation in which the lighter portions of the gray vertical scale correspond to higher regions of the surface and the darker portions to lower regions of the surface. The image in Figure 1 is composed of a hexagonal pattern of bright spots. This is the only periodic feature found on such samples and is routinely observed in our laboratory with both AFM and STM.[4] The average nearest-neighbor distance, which is represented by the black line (a) overlaying a small portion of the image, is 0.29 ± 0.03 nm. This distance agrees well with the 0.288-nm nearest-neighbor spacing of the (111) face of gold,[26] as found in earlier atomic scale images of mica-supported gold.[9a,b,d,e] Larger area scans show that the (111) periodicity extends over hundreds of square nanometers. On the basis of the combined weight of these and previous characterizations (see the Experimental Section), we will refer to our gold substrates simply as Au(111).

III. AFM Images of Alkanethiolate Monolayers at Au(111). Figure 2 shows images of alkanethiolate monolayers at Au(111) of three different chain lengths: (A) octadecanethiolate (n = 17); (B) decanethiolate (n = 9); (C) hexanethiolate (n = 5). Each image is presented with the same horizontal length scales as those in Figure 1. In all three images, a hexagonal pattern of bright spots with similar spacings is observed, the only periodic image observed to date for these films. These spacings are markedly larger than those of uncoated Au(111). The average respective nearest- and next-nearest-neighbor distances, which are represented by the black lines in Figure 2A, equal 0.52 ± 0.03 and 0.90 ± 0.04 nm for n = 17, 0.50 ± 0.02 and 0.91 ± 0.04 nm for n = 9, and 0.51 ± 0.02 and 0.92 ± 0.06 nm for n = 5. We have obtained images with similar spacings and uncertainties for alkanethiolate monolayers for the remainder of the series from n = 4 to 17. These distances correspond to those expected for a $(\sqrt{3} \times \sqrt{3})R30°$ adlayer on a Au(111) lattice, the same two-dimensional arrangement that has been found for these monolayers using diffraction[1-3] and STM techniques.[4,5] For illustration,[28] a scale drawing of the $(\sqrt{3} \times \sqrt{3})R30°$ adlayer on Au(111) is shown.

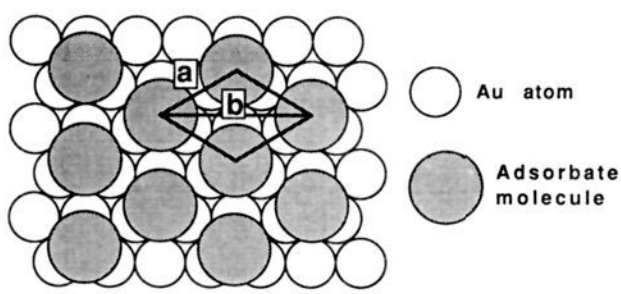

Figure 3 presents larger area images (8.45 nm × 8.45 nm) of the three monolayers shown in Figure 2. As previously noted, areas with a hexagonal pattern extend over a large portion of each image. The ordered areas, which are occasionally as large as 100 nm^2, are separated by regions of poor definition which vary in size. In contrast, areas as large as 600 nm^2 have been observed using STM.[4] Though tempting to ascribe these findings to differences in the long-range order (i.e., domain size) of the head group relative to the alkyl chains, more extensive large-area scanning is needed before such a conclusion could be reached. Larger area scans may also reveal possible correlations between domain sizes and chain length, as suggested by He diffraction,[1] a technique which probes the two-dimensional arrangement of

(25) For an overview of the spatial and conformation arrangement of these monolayers, see refs 13a,b and 14a. Detailed discussions on temperature effects can be found in refs 1 and 18d. Recent molecular dynamics simulations (Hautman, J.; Klein, M. *J. Chem. Phys.* **1990**, *93*, 7483–92) have also revealed the accumulation of thermally activated conformational disorder at the chain terminus.

(26) Kittel, C. *Introduction to Solid State Physics*, 5th ed.; Wiley: New York, 1976.

(27) The slight distortion in the image is attributed to thermally induced drift.

(28) The distances labeled in the adlayer scale drawing indicate the nearest- and next-nearest-neighbor spacings (a and b, respectively) of 0.50 and 0.87 nm, respectively, for an adsorbate forming a $(\sqrt{3} \times \sqrt{3})R30°$ adlayer on Au(111). Assuming each adsorbate binds at an equivalent site, identical $(\sqrt{3} \times \sqrt{3})R30°$ overlayer structures can be constructed at the 3-fold hollow sites, 2-fold bridging sites, or on-top sites. The 3-fold hollow sites are the most likely candidates as suggested by: (a) Reference 2a. (b) Ogletree, D. F.; Ocal, C.; Marchon, B.; Somorjai, G. A.; Salmeron, M.; Beebe, T.; Siekhaus, W. *J. Vac. Sci. Technol. A* **1990**, *8*, 297–301. Recent ab initio calculations also point to the 3-fold hollows as the preferred site: Ulman, A. Eastman Kodak Co. Private communication.

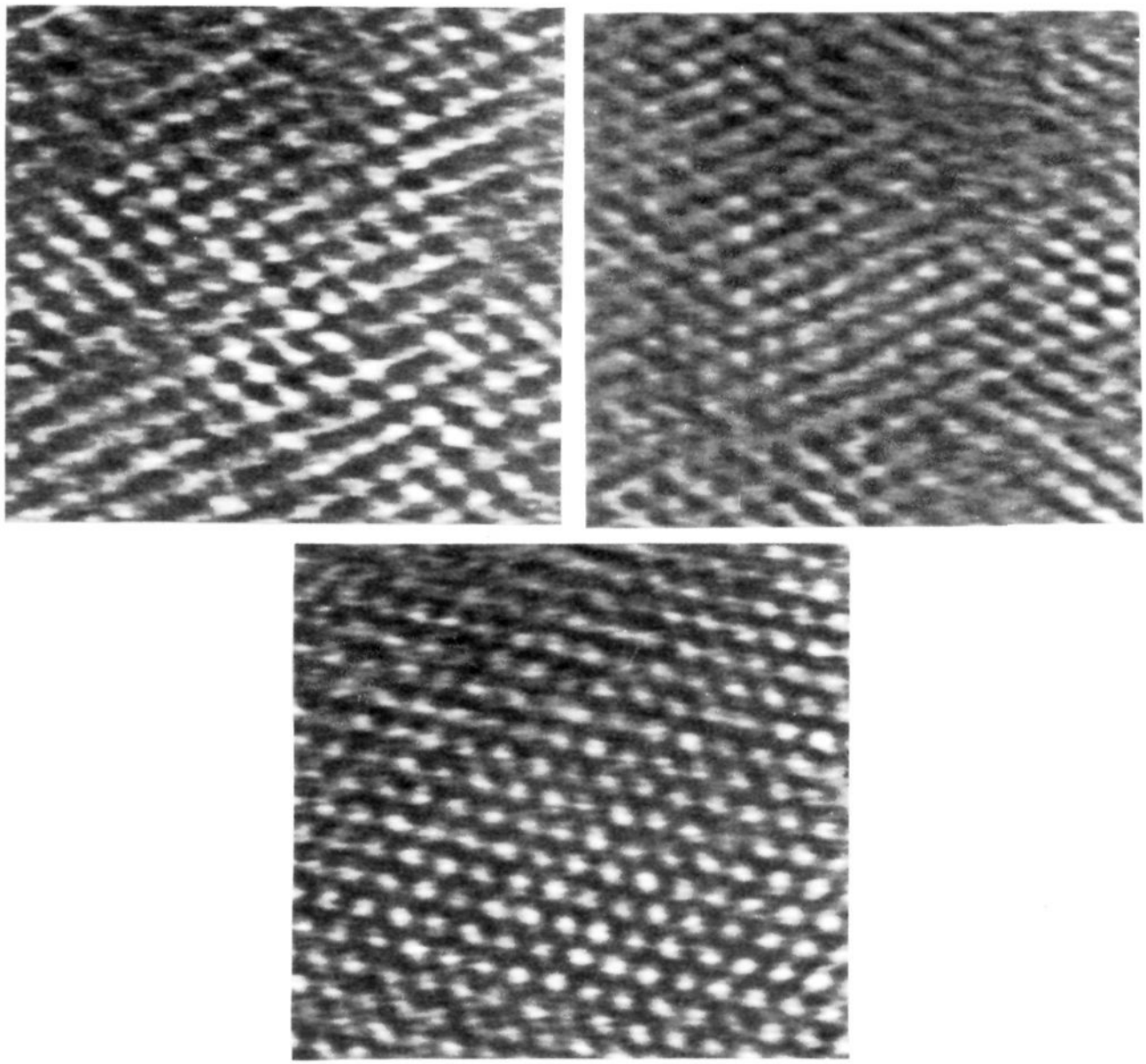

Figure 3. AFM images covering 8.45 nm × 8.45 nm of (A, top left) octadecanethiolate, (B, top right) decanethiolate, and (C, bottom) hexanethiolate at epitaxially grown Au(111). Images A and B were low-pass filtered, and C was filtered lightly with an XY spectrum filter.

the terminal methyl groups of these monolayers.

Taken together, the images in Figures 2 and 3, which are representative of findings from several hundred hours of scanning, demonstrate the capability of AFM to image alkanethiolate monolayers at gold surfaces with atomic scale resolution. The images further reveal that these thiolates form a $(\sqrt{3} \times \sqrt{3})R30°$ adlayer on a Au(111) lattice, in agreement with the noted diffraction[1-3] and STM[4,5] findings. This structural arrangement is also consistent with the chain tilts deduced by infrared spectroscopic characterizations[13b,14a,29] and with surface coverages determined from electrochemical reductive desorption[12a,19] measurements, approaches that probe macroscopic details of interfaces.

IV. Imaging Mechanism. To develop a structural interpretation of our images, it is important to determine the position of the AFM tip with respect to the sample surface. Such a determination would effectively identify the portion of the monolayer structure that is probed by the AFM tip (e.g., chain terminus or gold-bound thiolate). Model calculations have suggested that representative images of surfaces of individual biological macromolecules can be obtained only if the force between the AFM tip and sample is on the order of 0.01 nN.[30] Above this limit, the tip may deform the surface of the sample. We believe that both the strong cohesive interactions operative within the array of alkyl chains and the covalent linkage between the sulfur head group and the gold surface enable our alkanethiolate monolayers to withstand much larger imaging forces. These factors were not taken into account in the noted calculations.

Several literature precedents support the importance of both of the above factors in imaging with AFM. With respect to cohesive interactions, the recent atomically resolved images of a multilayer cadmium arachidate film[10a] and of other Langmuir–Blodgett-deposited films[11a] are particularly noteworthy. The images in both studies were acquired at ~10 nN. Force–distance profiles measured as an AFM tip approaches, contacts, and then penetrates into a film of cadmium arachidate[15] are in general accordance with these findings, with penetration occurring at ~7 nN. The importance of a strong linkage between an ordered overlayer and the support has been illustrated in recent friction and wear studies of multilayer films of cadmium arachidate at

(29) Walczak, M. M.; Chung, C.; Stole, S. M.; Widrig, C. A.; Porter, M. D. *J. Am. Chem. Soc.* **1991**, *113*, 2370–8.

(30) Persson, B. N. *J. Chem. Phys. Lett.* **1987**, *141*, 366–8.

the native oxide of a silicon substrate.[17] These studies found that the first layer, which is tethered to the oxide via acid-base chemistry, is ~1000 times more resistive to wear than the subsequent layers held together primarily by van der Waals forces. Together, the above results attest to the ability of organic films with structures similar to alkanethiolate monolayers to withstand forces similar to those used to acquire our images.

As stated previously, we attribute our images to interactions between the AFM tip and the alkyl chain structure of the monolayer. This conclusion, supported by the above literature findings,[10a,11a,15-17] is based on the differences in the capabilities of AFM and STM to image the atomic structure of short-chain ($n \leq 3$) alkanethiolates at Au(111). With STM,[4] for example, we have routinely obtained atomically resolved images of ethanethiolate ($n = 1$) monolayers. We have ascribed these images to electrons tunneling between the STM tip and the gold surface through the sulfur head group, placing the STM tip near the gold surface. If the AFM tip images the gold-bound sulfur, one would then reasonably expect to obtain images with the hexagonal pattern for all chain lengths,[31] not only for $n \geq 4$. This result argues that the atomically resolved images of the longer chain ($n \geq 4$) monolayers arise from interactions between the AFM tip and the alkyl chain structure. The aforementioned chain length dependence of the range of forces that gave atomically resolved images is consistent with this interpretation. Interestingly, the inability to obtain images for $n \leq 3$ further suggests that most likely position of the AFM tip to be near the outermost carbons of the alkyl chains. However, it is not clear if the tip probes the packing arrangement of the chain terminus or pushes through the first few carbons and images the underlying polymethylene chain structure. The latter possibility may have relevance to the inability to obtain atomically resolved images of the short-chain ($n \leq 3$) monolayers (i.e., the tip induces disorder). The inherent disorder of the short alkyl chain structures[1,13b,14a,18c,d] may also be a contributing (and possibly the dominant) factor. We are currently designing experiments in an attempt to resolve these issues.

(31) This contention is further supported by recent electrochemical measurements of surface coverage.[12,19] These studies found that the surface coverage of alkanethiolate monolayers at Au(111) is constant from $n = 2$ to 17. We also note that the measured coverage of $(8.4 \pm 0.7) \times 10^{-10}$ mol/cm^2 compares reasonably well with the 7.6×10^{-10} mol/cm^2 coverage expected for a $(\sqrt{3} \times \sqrt{3})$R30° adlayer on Au(111).

Conclusions

This paper has demonstrated that it is possible to resolve atomic scale features of organic monolayer films at gold using AFM under ambient laboratory conditions and reaffirms the presence of a $(\sqrt{3} \times \sqrt{3})$R30° adlayer structure for alkanethiolate on Au(111). This and other recent findings suggest that AFM may prove valuable in providing detailed microscopic information for developing insights into interfacial structure-reactivity relationships. Both cohesive interactions between neighboring chains and the covalent linkage between the sulfur head group and gold surface have been identified as factors that play an important role in the ability to obtain these images. Experiments are in progress to evaluate further the capability of this technique to reveal the structure of various other monolayer films. We are particularly interested in developing further insight into the AFM imaging mechanism to facilitate a detailed comparison of our findings with those from He diffraction,[1] noting the possible complementary nature of the information supplied by the two methods. Extension to characterizations under thin layers of contacting liquids is also under way.

Acknowledgment. M.D.P. gratefully acknowledges the support of a Dow Corning Assistant Professorship. We thank Dr. Vickie Hallmark for invaluable advice on the preparation of the mica-supported gold substrates and Professors Cindra Widrig and Duane Weisshaar for helpful discussions. The synthesis of pentadecanethiol and tridecanethiol by Professor Chinkap Chung is appreciated. We thank Professor Allen Bard and Dr. Abraham Ulman for communicating their preliminary findings. Ames Laboratory is operated for the U.S. Department of Energy by Iowa State University under Contract No. W-7405-eng-82. This work was supported by the Office of Basic Energy Sciences, Chemical Science Division.

Registry No. Au, 7440-57-5; $CH_3(CH_2)_nSH$ ($n = 1$), 75-08-1; $CH_3(CH_2)_nSH$ ($n = 2$), 107-03-9; $CH_3(CH_2)_nSH$ ($n = 3$), 109-79-5; $CH_3(CH_2)_nSH$ ($n = 4$), 110-66-7; $CH_3(CH_2)_nSH$ ($n = 5$), 111-31-9; $CH_3(CH_2)_nSH$ ($n = 6$), 1639-09-4; $CH_3(CH_2)_nSH$ ($n = 7$), 111-88-6; $CH_3(CH_2)_nSH$ ($n = 8$), 1455-21-6; $CH_3(CH_2)_nSH$ ($n = 9$), 143-10-2; $CH_3(CH_2)_nSH$ ($n = 10$), 5332-52-5; $CH_3(CH_2)_nSH$ ($n = 11$), 112-55-0; $CH_3(CH_2)_nSH$ ($n = 12$), 19484-26-5; $CH_3(CH_2)_nSH$ ($n = 13$), 2079-95-0; $CH_3(CH_2)_nSH$ ($n = 14$), 25276-70-4; $CH_3(CH_2)_nSH$ ($n = 15$), 2917-26-2; $CH_3(CH_2)_nSH$ ($n = 16$), 53193-22-9; $CH_3(CH_2)_nSH$ ($n = 17$), 2885-00-9.

Intrinsic (Gas-Phase) Basicity of Some Anionic Bases Commonly Used in Condensed-Phase Synthesis

Deborah Thomas Grimm† and John E. Bartmess*

Contribution from the Department of Chemistry, University of Tennessee at Knoxville, Knoxville, Tennessee 37996-1600. *Received May 20, 1991*

Abstract: The gas-phase acidities of a number of alkylamines and alkylsilanols, used widely in organic synthesis, have been determined. They fall in the expected order based on polarizability, but the value for hexamethyldisilazane is anomalous. It is a considerably stronger acid in the gas phase, relative to other common functional groups, than in solution. The disilazide anion cannot deprotonate ketones in the gas phase, while it does so readily in solution. This is attributed to the effect of the lithium counterion in solution.

There are a variety of strong anionic Brønsted bases, such as butyllithium, lithium diisopropylamine, potassium hydride, etc., commonly utilized for deprotonation of substrates. Chemists tend to use the strongest base available to ensure deprotonation on the first attempt, with modification to reduce nucleophilicity only when necessary.[1] In the usual solvent systems employed for such work, however, the nature and concentration of the counterion,[2] solvent,

† Current Address: Coordinated Instrument Facility, 604 Lindy Boggs Hall, Tulane University, New Orleans LA 70118-5698.

(1) d'Angelo, J. *Tetrahedron* **1976**, *32*, 2979. House, H. O. *Modern Synthetic Reactions*, 2nd ed.; Benjamin: Menlo Park, CA, 1972; Chapter 9.

0002-7863/92/1514-1227$03.00/0